Distributions Across the Plume of Transverse Liquid and Slurry Jets in Supersonic Airflow

R.H. Thomas* and J.A. Schetz†
Virginia Polytechnic Institute and State University, Blacksburg, Virginia

Liquid and slurry jets were injected through a circular orifice transverse to a $M = 3$ airflow. Mass samples of both jets were taken across the plume 30 injector diameters downstream. Pitot and static pressure surveys were taken across the liquid jet. These data allowed the calculation across the liquid jet plume of the Mach number, air mass flow, liquid-to-air ratio, and momentum flux. In the center third of the plume area, there is a core region of subsonic airflow that carries two-thirds of the mass collected in the plume. In the core, the liquid mass flow is nearly constant from side to side at a given height and the average velocity of the liquid is only 30-60% of the local air velocity. A supersonic mixing region surrounds the core region. Comparison with these direct sampling results indicate that correlations developed from photography are inadequate in determining the penetration and width of either jet. The slurry jet showed substantial phase separation. When a 30% mass-loaded slurry of 1-5 μm silicon dioxide particles mixed with water was injected, the local loading varied from a low of 13% at the bottom of the plume to 100% outside the plume.

Nomenclature

C_a = air concentration in plume
C_d = discharge coefficient
C_l = liquid concentration in plume
C_{l_m} = liquid concentration on the centerline
d = injector diameter
h = penetration of jet plume
h_{core} = penetration of jet plume core
M = Mach number
$\dot{m}_a/A$ = mass flow of air per unit area
$\dot{m}_l/A$ = mass flow of liquid per unit area
P_s = static pressure
P_{t1} = local freestream total pressure
P_{t2} = local pitot pressure
$\bar{q}$ = jet to freestream momentum ratio
R = gas constant for air
T_0 = local total temperature
T_s = local static temperature
V_j = injectant velocity at injector
V_∞ = freestream velocity
V_l = average velocity of liquid in plume
V_a = local velocity of air in plume
w = width of jet plume
w_{core} = width of jet plume core
x, y, z = rectangular coordinates, origin at injector
y_c = distance from centerline to y at $C_l = \frac{1}{2} C_{l_m}$
ρ_∞ = free stream density
ρ_j = injectant density
γ = ratio of specific heats

Introduction

THE study of jets injected transverse to a supersonic gas crossflow is a problem of both practical and theoretical interest. Such a process is encountered in thrust vector control, local re-entry body cooling, external burning on projectiles, control of vehicles, and fuel injection into supersonic combustion chambers. Theoretical interest is derived from the complexity of the general problem, including three-dimensional, multiphase, unsteady, turbulent flow with subsonic and supersonic regions. Some applications also involve chemical reactions. This complexity makes it prohibitive at this time to approach the problem from an entirely theoretical point of view requiring extensive basic experimental studies.

Much work has been done to develop correlations for jet penetrations that include the effect of the injection angle.[1-4] All of these investigations used photography to determine the penetration, but they did not establish how accurately such pictures represented the actual penetration. The effect of liquid viscosity and surface tension on the penetration were found to be minimal.[5] However, Nejad and Schetz[6] determined that these properties did affect the droplet diameter. Many injector configurations were tested by Joshi and Schetz[7] to determine the effects on penetration and spread. The improved atomization from those injector combinations producing impinging jets has been documented by Hewitt and Schetz.[8] The actual process by which these jets break up and atomize has been observed by Joshi et al. to be a gross clump fracture.[9,10] These investigations, along with other work, have concentrated on the penetration, atomization, structure, and breakup of liquid jets.

Fuels more energetic than conventional liquids have always been under consideration because of potential gains in range and compactness. One attractive alternative is slurry fuels produced by suspending metal powders in hydrocarbon liquids. The possible increase in the heat of combustion is significant.[11] Olson and Breitwiser[12] describe many of the results of early NACA research in slurry fuels. The difficulty of boron slurry combustion was made evident. At locally rich fuel-air ratios, high local gas temperatures resulted in the destruction of combustors; however, at cooler temperatures, significant deposition of boron oxides resulted along with unacceptably low combustion efficiencies.

Reference 13 describes recent advancements in boron combustion. Less and Schetz[14] have studied the injection of slurry fuels, examining the penetration and breakup of slurry jets injected transverse to a supersonic stream. They observed photographically that there was significant phase separation.

Presented as Paper 84-0041 at the AIAA 22nd Aerospace Sciences Meeting, Reno, NV, Jan. 9-12, 1984; received June 27, 1984; revision received March 1985.

*Graduate Assistant, Department of Aerospace and Ocean Engineering. Student Member AIAA.

†Professor and Chairman, Department of Aerospace and Ocean Engineering. Fellow AIAA.

Good mixing of the fuel and air is important for efficient combustion in any system, but proper mixing of any type of fuel with the main airflow is imperative in supersonic combustion because of the low residence times. This is the problem of interest here and the understanding of it is linked to a fundamental knowledge of the jet structure, breakup, and plume characterizations. The previously mentioned research has contributed to the understanding of jet structure and breakup. However, distributions of important quantities in the plume has been sparsely researched. Chinese researchers have determined, by direct sampling, fuel distributions for liquid transverse injection in subsonic streams.[15] Soviet researchers, indirectly using a temperature survey method, determined the gas-phase concentration inside a liquid jet injected transverse to a supersonic stream.[16] Thus, the present research was designed to determine the first mass distribution by direct sampling in both a liquid and a slurry jet in supersonic airflow. The mass distribution combined with static and pitot pressure measurements could then be used to calculate other important distributions in the jet plume. In addition, this information combined with new photographic observations provides further insight into the basic fluid mechanics of this complex problem.

Experimental Apparatus and Methods

Test Facility

Eight hundred tests were conducted in the Virginia Tech 23×23 cm supersonic blowdown wind tunnel. All tests used the Mach 3 configuration. The stagnation pressure was maintained at 4.5 atm $\pm$ 2% and the stagnation temperature was that of outside ambient air ($\sim 25°C$). Run times were at least 15 s.

Injectant

Cost and safety considerations prohibited using hydrocarbon carriers and solid fuels such as boron in this work. Water was used to simulate hydrocarbon fuels and a mixture of water and silicon dioxide particles served as the slurry. No additives were included in the slurry mixture. The use of substitute injectants such as these are accepted practice for basic studies. The silicon dioxide particles have a density of 2.35 g/ml and are of irregular shape, thus approximating elemental boron. The particles were manufactured to a size range of 1-5 μm by Atlantic Equipment Engineers.

Injection System

A modified 6 liter chemical mixer was used to insure uniform mixing of the slurry. The tank was pressurized to 12 atm for slurry injection with continuous mixing throughout the run. For water injection, the mixer was used as a reservoir pressurized to 17 atm.

Flat-Plate Model

The liquid and slurry were injected through a flat plate having dimensions $10.0 \times 15.25 \times 0.9$ cm and a sharp leading edge. The circular injector orifice was located 8.0 cm downstream of the leading edge. The orifice had a conical entry passage and a diameter of 2.0 mm. It was the intent of this research to simplify this flow problem as much as possible by studying a basic configuration that could later be extended. Thus, the flat-plate model was used to minimize the boundary layer and its effects.

Photographic Methods

Two types of photographs were taken. First, a General Radio Strobotac was used as the light source for a schlieren optical apparatus to take spark schlieren photographs. The 10^{-6} s exposure time with type 57 Polaroid (ASA 3000) film provided an instantaneous shock shape and side view of the jet. Second, front-lighted photographs provided unique views of the jet leading edge. Exposure times of 10^{-4} s were used on Ektachrome ASA 64 film and were used with a commercially available Minolta X-700 35 mm camera with a Minolta 360 PX flash.

Sampling System

The sampling probe was designed to obtain true mass flow samples at supersonic speeds. The probe was connected to a vacuum system that created a pressure inside the probe lower than the total pressure behind the stand-off shock in front of the probe, causing the shock to be swallowed into the probe. In this fashion, a stream tube equal in area to the probe capture area can enter the probe undisturbed. The internal probe diameter diverged from 1.2 to 5.1 mm, causing one normal shock in the sampling tube (see Fig. 1). A 45 cm run of 5.1 mm i.d. tubing took the sample from the capture area to a three-way valve outside the tunnel. The valve switched the sampling flow between a dummy sample bottle and a true sample bottle. The vacuum system established flow through the dummy bottle until steady conditions were reached. The valve then switched the sampling flow to the true sampling bottle for 5 s and then back to the dummy well before any end-of-run transients. This allowed the mass flow of injectant for the given probe capture area to be calculated. The sampling system is shown in Fig. 2. A side-view spark schlieren photograph (see Fig. 3) shows the probe in operation as described.

Liquid jet samples were collected in 15 ml plastic bottles weighing approximately 5 g; in the slurry tests, 15 ml glass bottles weighing 13 g were used. Each bottle was tared on a Mettler 33AR precision balance accurate to ± 0.0005 g.

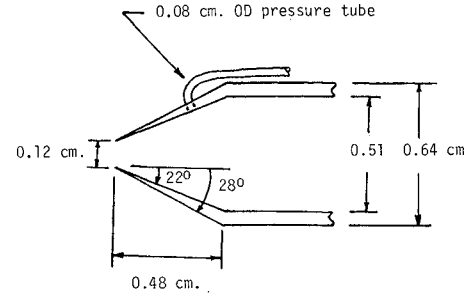

Fig. 1 Sampling probe.

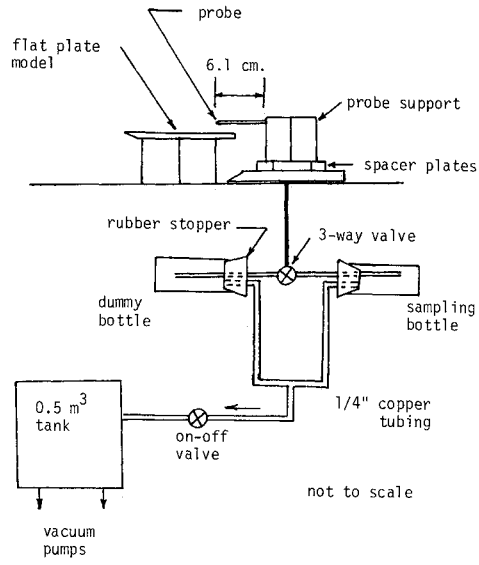

Fig. 2 Sample collection system.

Slurry samples were weighed wet and then heated at 105-130°C to evaporate all of the liquid and then weighed again to determine the solid weight.

On the periphery of the slurry jet—where solid particles had been thrown free of the jet—a filter system replaced the sample bottle. These were glass fiber Gelman Sciences filters of 0.7 μm pore size used in a Gelman 1190 filter holder.

Pressure Measurements

The pressure tap in the sampling probe was primarily intended to check the flow conditions during sampling. The probe could also be used as a pitot pressure probe. In supersonic flow, the pressure measured was then the total pressure behind the normal shock in front of the probe, P_{t2}. This also permitted the determination of when the vacuum system could lower the pressure in the probe below this value in order to insure the swallowing of the shock. However, due to the erosive slurry, the sampling probe had to be replaced four times and the pressure tap was also moved to the sampling bottle area.

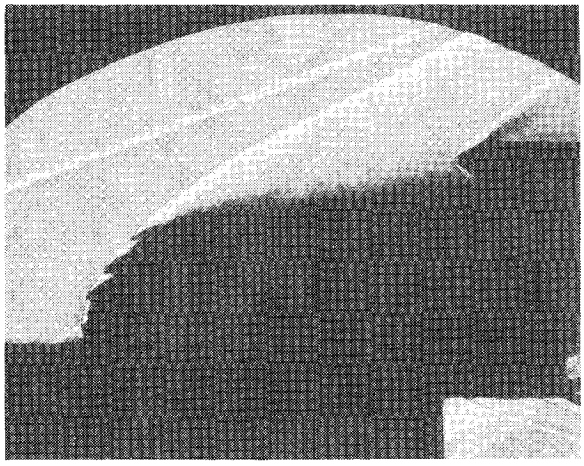

Fig. 3 Spark schlieren photograph of $\bar{q} = 6.0$ liquid jet.

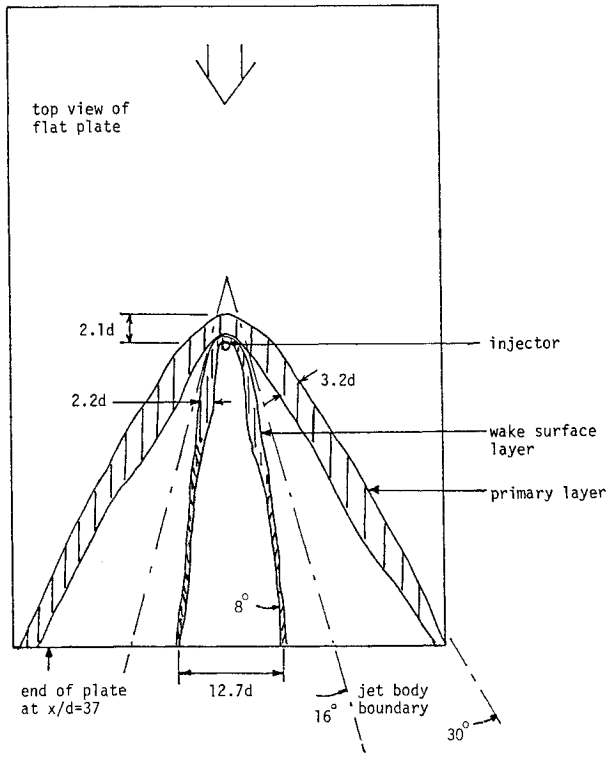

Fig. 4 Surface erosion pattern of $\bar{q} = 6.0$ liquid jet.

A small flat plate 1.27 × 1.91 × 0.16 cm with a pressure tap on the surface and a sharp leading edge was used to measure the static pressure in the liquid jet only. Thus, at each station, the total pressure behind the shock P_{t2} and the static pressure P_s could be measured. If the flow was not supersonic, the total pressure measured would be P_{t1}, the local freestream total pressure.

Test Matrix and Parameters

The primary similarity parameter used in injection studies is $\bar{q}$, $(\rho_j V_j^2/\rho_\infty V_\infty^2)$. A $\bar{q} = 6$ was chosen for the liquid jet tests and was maintained to within ±1.7%. The corresponding mass flow rate was maintained at 90 g/s ± 1.1% throughout.

A right-handed coordinate system was used with the origin at the injector; the x coordinate running downstream and z coordinate perpendicular to the flat plate were used to present the data. All of the data were collected in the $x/d = 30$ plane. Previous work has concluded that penetration due to jet normal momentum is complete at this downstream station.[9,16] Samples were taken in the $-y/d, z/d$ half-plane at increments of $2d$ for the bulk of the data. Traverses at three values of z/d in the $+y/d$ plane were made to check for jet symmetry. At each station, at least three samples were taken.

The solid loading of a slurry is defined as the mass of the solid divided by the mass of the total mixture. A loading of 30% was chosen as a reasonable value for an exploratory study. Higher loadings (> 55%) produce complex changes in the injectant flow from the orifice (see Ref. 14), and it was decided to avoid those complexities in this work. The loading of 30% corresponds to a mixture density of 1.208 g/ml that was maintained to within ±1.5%. Since mass distributions were to be collected, it was felt that the mass flow of the slurry should be matched with the liquid tests. For the slurry tests, the mass flow was maintained at 90 g/s ± 6.6% corresponding to $\bar{q} = 5 \pm 14.0\%$.

Again, most slurry sampling was done in the $-y/d, z/d$ half-plane with two traverses in the $+y/d$ half-plane to check for symmetry. At least two samples were collected at each

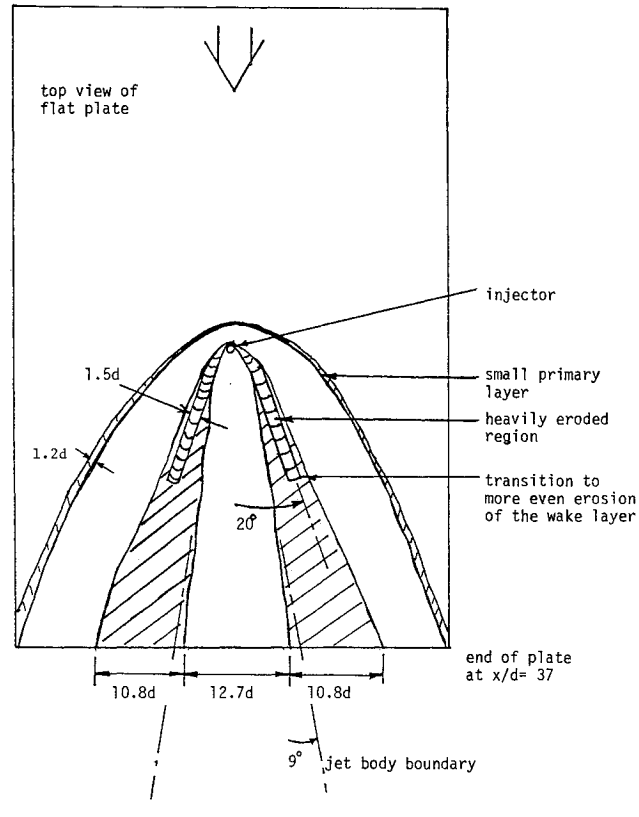

Fig. 5 Surface erosion pattern of $\bar{q} = 5.0$ slurry jet.

station. Greater margins in the flow rate were allowed and fewer samples were collected in the slurry jet survey due to the increased cost and difficulty of these tests.

Results

Surface Layer

The surface layer is created by the interaction of the separation region around the injector, the boundary layer, and the jet column. On the surface of the flat plate, liquid is drawn upstream for a short distance directly in front of the leading edge of the jet column. This liquid is then split into two strands that are swept downstream far on either side of the jet. Top view photography has documented this primary surface layer.[7]

Front-lighted photographs on liquid injection at $\bar{q} = 6.0$ clearly show the primary surface layer, but also show a substantial layer directly underneath the jet. Reference 9 just mentioned the existence of this "wake" surface layer. Hundreds of runs at the same conditions were required in order to accomplish the mass flow distribution to be described and the result was that polished surfaces were left by the surface layer. These are sketched in Fig. 4. The measured width from the mass distribution at $x/d = 30$ is $20d$ and using this with the observation that the half-angle of divergence is 16 deg, which is roughly constant for liquid jets of $\bar{q} > 4$,[9] the rough boundary of the jet from the top view is sketched in Fig. 4. It clearly shows that the wake surface layer is obscured by the jet body and plume. Previous researchers[7,9] have used only top-view photography to observe the layer and, thus, this has gone undocumented. The half-angle of divergence of the two strands that made up the wake layer is 8 deg or half that of the main jet body.

A much more defined pattern is documented in Fig. 5 after 100 runs at $\bar{q} = 5$ because of the more erosive nature of the slurry. Only a trace of a primary layer was noticed in contrast to the larger primary layer of the liquid jet. However, a relatively heavily eroded region corresponded to the wake layer. Again, using the known width at $x/d = 30$, the half-angle of divergence of the slurry jet can be no more than 9 deg. This is in sharp contrast to the relatively constant 16 deg found for liquid jets. Furthermore, the half-angle of divergence of the wake layer was 20 deg, more than twice that for the liquid jet.

The front-lighted photographs also show that there is considerable transfer of mass from the plume to the surface downstream of the injector. This, together with the significant erosion patterns, appears to indicate that a significant percentage of the injected mass flow may be carried in the surface layer.

Jet Leading Edge

Previous research has shown that high-frequency, large-amplitude, aerodynamically induced waves that ultimately result in gross fracture of the jet body begin to grow on the leading edge soon after exiting the injector.[9] Front-lighted photographs show a cone-shaped liquid core just at the exit of the injector. Its height is about one injector diameter. At this height, liquid begins to be sheared off the sides of the jet to form spray. However, a leading edge remains liquid for an additional 3-4d for a total height of 4-5d. This is the leading-edge wave strip where the waves mentioned above form. The strip is obscured on either side and beyond a height of 4-5d by spray and/or clump formation. Pictures of the slurry jet do not reveal the core or wave strip. However, this is probably due to the low contrast between the opaque, white slurry and the white-appearing spray. More discerning visual observations indicate that the slurry exhibits a similar structure.

The height of the wave strip is also close to the sonic angle location for these conditions. The sonic angle is defined as that point on the bow shock immediately downstream of which the flow is sonic. This occurs since the bow shock is initially normal; as the jet is turned by the flow, the bow shock becomes oblique. The transition to supersonic flow changes the wave nature on the jet to a longer wavelength type that later produces the jet body fracture.[9] The jet body is the continuous liquid portion of the jet before fracture produces the spray plume. This transition obviously creates a spray that obscures the wave strip as seen in the front-lighted photographs. At $M = 3$ the sonic angle is 64 deg. The vertical distance to the location of the sonic angle was in the range of 5-6d from spark schlierens such as Fig. 3.

The combined picture of a wave strip with surface wave growth and spray formation off the sides of the jet indicate that perhaps a circulation pattern in a kidney-shaped cross section exists similar to that documented in transverse jets in subsonic flow.[17] This pattern might persist downstream and be noticeable in the plume distributions to be presented shortly.

Liquid Sampling

The results of the sampling for the liquid jet case are presented in Fig. 6 in terms of mass flow per unit area ($g/s \cdot mm^2$). Shown is one-half of the $x/d = 30$ plane of the jet.

The actual cross-stream penetration of the jet at this station and how it compares with penetration estimates as compiled from photographic techniques is the first result. It can be seen that trace amounts of samples were collected at 19 injector diameters high, but, considering these as negligible, $z/d = 18$ could be called the penetration. Samples at $z/d = 18$ are roughly 4.0% of the maximum sample size on the centerline $y/d = 0$. Yates and Rice[1] obtained the following empirical equation for water penetration from a circular injector into a

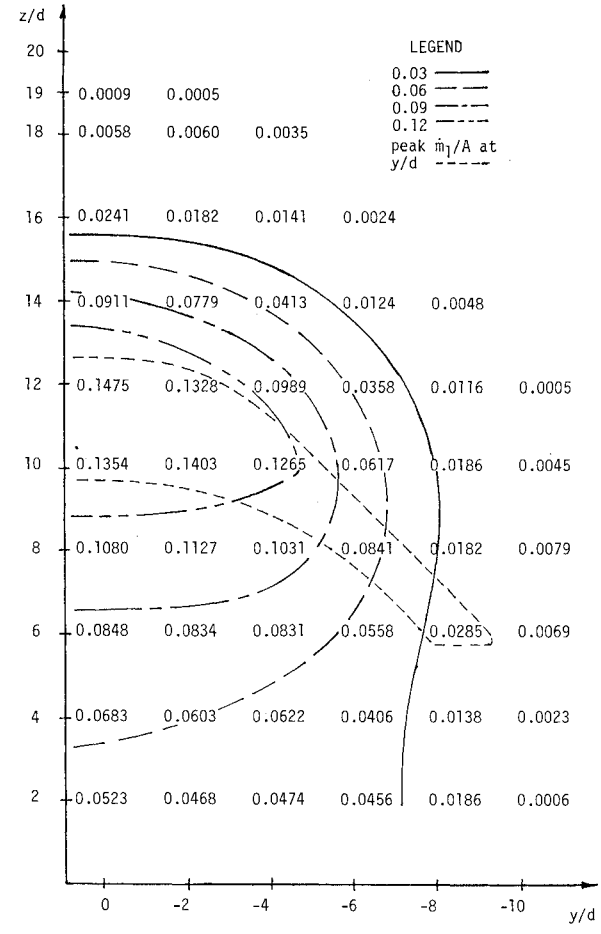

Fig. 6 Mass flow of liquid per unit area, $\dot{m}_l/A$ in $g/s \cdot mm^2$, for $\bar{q} = 6.0$ jet at $x/d = 30$. Peak $\dot{m}_l/A$ region is the remnant of the kidney-shaped main jet body.

Mach 3 cross flow:

$$h/d = 1.15(\bar{q})^{\frac{1}{2}} \ell n[1 + 6x/d]$$

At $x/d = 30$ and $\bar{q} = 6$, this yields $h/d = 14.6$ or 19% below the actual penetration of $h/d = 18$. It can be noted that the point of maximum $\dot{m}_l/A$ is $z/d = 12$ or two-thirds the value of maximum penetration. Figure 6 also allows the width of the jet at $z/d = 30$ to be determined. The data show that by $y/d = -10$, $\dot{m}_l/A$ is generally under 6% of the centerline value at that value of z/d. Joshi and Schetz[7] give the following expression for jet width:

$$w/d = 11.2(\bar{q}C_d)^{0.19}$$

with an insignificant pressure term ignored. For circular injectors, $C_d \simeq 1.0$, and $\bar{q} = 6$, Joshi's formula yields $w/d = 15.8$ or 21% below the present value of $w/d = 20$. Thus, photographic techniques seriously underestimate the plume dimensions. This compares favorably with the results of Ref. 18, which concluded that the error in determining the plume boundary from photographic techniques could be 25-30%. Using a temperature survey method, Ref. 16 presented the following correlations for jet penetration and width:

$$h/d = 3.75(\bar{q})^{0.414}(x/d)^{0.239}$$

and

$$w/d = 13.8(\bar{q})^{0.25} \text{ at } x/d = 30$$

These yield values of $h/d = 17.8$, which are negligibly different from the present value of 18 and $w/d = 21.6$ or 8% above the present value of 20. These values are in good agreement and demonstrate the importance of direct measurements.

From $z/d = 2$-10, the mass flow is relatively constant at each z/d station from $y/d = 0$ to -4 before dropping sharply toward the boundary. This identifies a core region with constant mass flow at a given z/d station. This core occupies approximately one-third the area of the jet plume. A region has been drawn in Fig. 6 that encloses the peak values of mass flow at each value of y/d. Apparently, this region is the now coflowing remnant of a kidney-shaped cross section in the jet body, indicating that such a cross section may exist, as postulated previously. Most of this region is within the plume core, implying that the jet body determines the characteristics of the plume core.

An integration of the mass flow across the $x/d = 30$ plane from the sampling data resulted in a mass flow of 67 g/s or 75% of the mass flow through the injector. As has been discussed, there is considerable evidence to indicate that the mass flow in the surface layer is a considerable portion of the remaining mass flow.

Liquid Jet Symmetry

Jet symmetry and repeatability of the results were checked carefully. Figure 7 shows the data at one z/d height. Data were taken in the $+y/d$ plane as well as some repeated sets of data in the $-y/d$ plane. Two other sweeps were done at $z/d = 10$ and 12. Two points can be made. First, when the data were repeated at a station (two separate three-sample sets), averages were within $\pm 10\%$ and the difference between the high and low values were generally overlapping. Second, these three sweeps show some asymmetry about $y/d = 0$, with symmetry about any other value of y/d not apparent.

Slurry Sampling

Figure 8 shows data taken in the $x/d = 30$ plane for the 30% loaded slurry jet. Both the average local loading of the samples and the total mass flow per unit area are shown. The loading increases smoothly in the $+z/d$ direction from $z/d =$ 2-10 and then jumps sharply at $z/d = 12$ to almost triple the value at $z/d = 2$. This increased loading is due to the heavier particles following paths with greater radii of curvature due to their greater inertia and thus separating from the plume consistent with the visual observations of Ref. 14. Perhaps unexpectedly, the same phase separation was noticed side-to-side in the $-y/d$ direction at both $z/d = 2$ and 10. The same trend was evident in the $+y/d$ direction. Some symmetry of the slurry plume about the centerline $y/d = 0$ is evident in mass flow and to a small extent in the loading.

Beyond the slurry jet boundary, samples of dry particles were collected using the filter system described previously. At $z/d = 14$ and $y/d = 0$, samples of negligible weight were collected on only one-third of the runs. At $z/d = 10$ and $y/d = +8$, samples were collected three-quarters of the time, but at $z/d = 10$ and $y/d = -8$, the rate was only one-fourth.

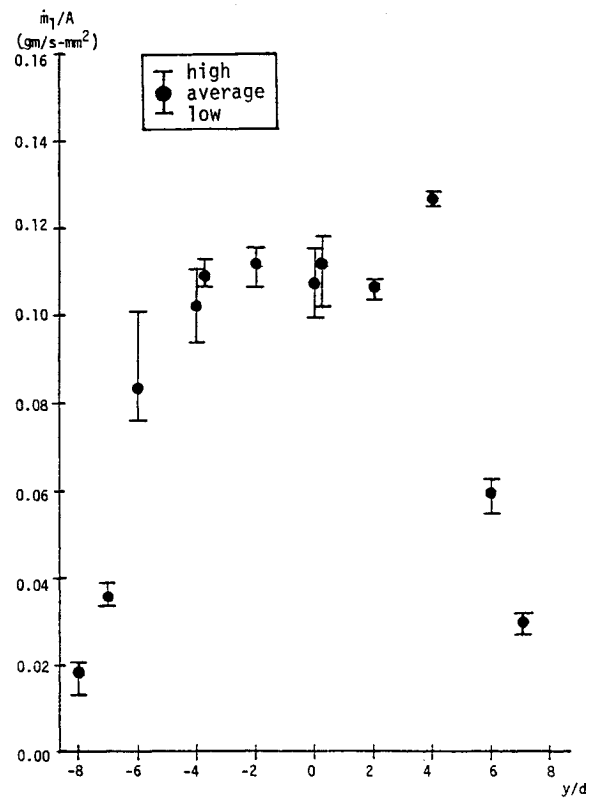

Fig. 7 Mass flow profile for the liquid jet at $z/d = 8$.

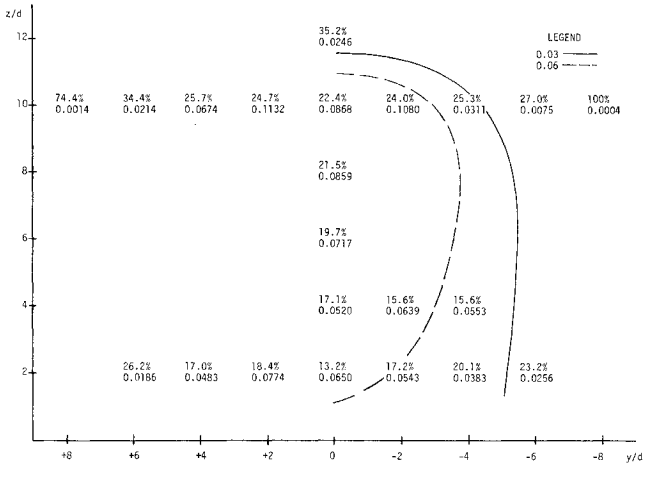

Fig. 8 Mass flow of slurry per unit area in g/s · mm^2 in the $x/d = 30$ plane of a $\bar{q} = 5.0$ slurry jet and the local loading in percent.

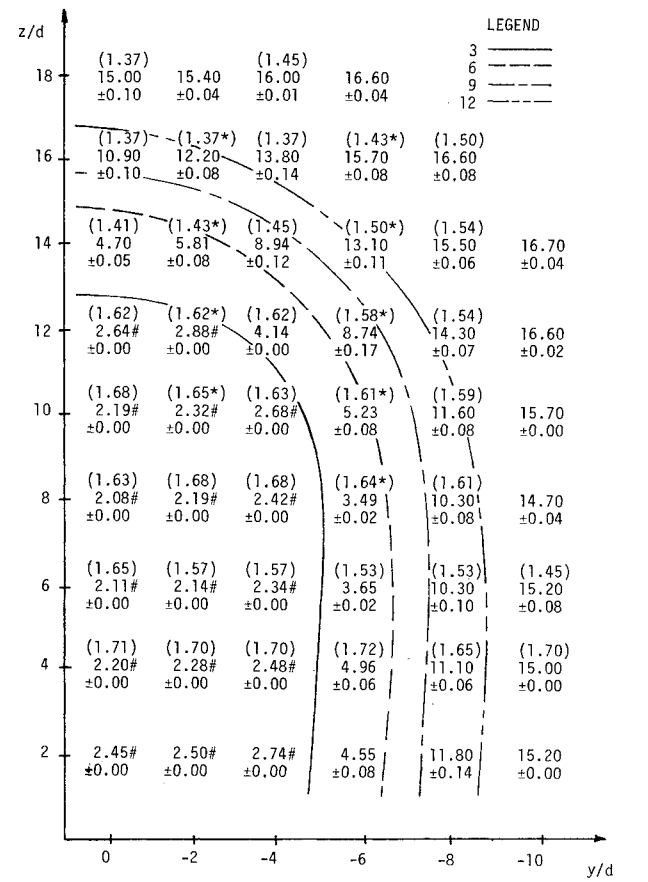

Fig. 9 Liquid jet pressures: pitot P_{t2}, # are P_{t1}, ±time variation in P_t values; P_s in parentheses; all pressures multiply by 10^4 N/m^2, (* denotes interpolated P_s values).

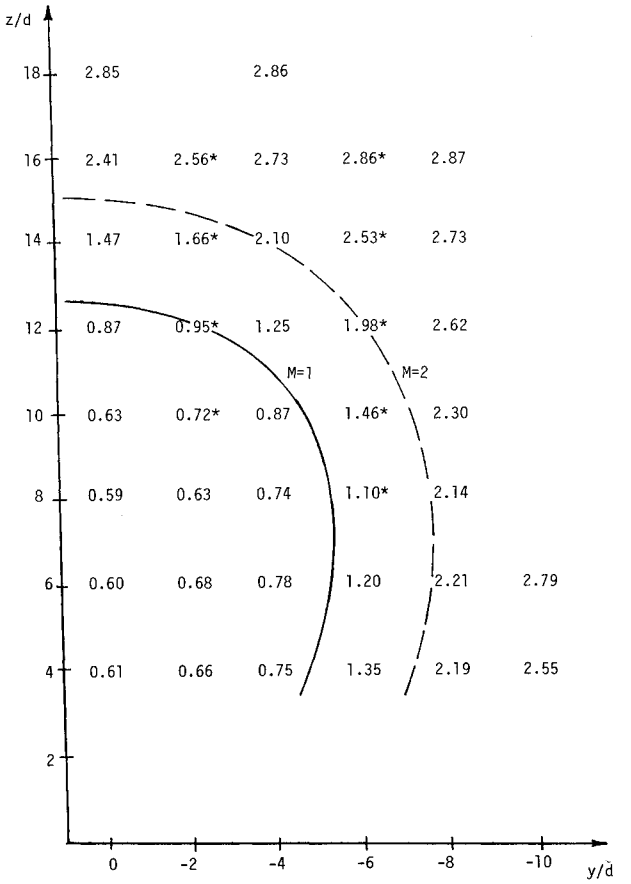

Fig. 10 Calculated Mach number distribution for the liquid jet (* denotes interpolated P_s values).

The sampling data define the penetration at $h/d = 12$. This is 13% below the Yates and Rice[1] correlation value of 13.6 for these conditions, although it must be considered that the correlation was developed for liquids only. Reference 14 determined the penetration for an identical slurry using photographs at $h/d = 13$, also high. However, solids alone will penetrate at least 16% higher, occasionally to $z/d = 14$. The width of the slurry jet, $w/d = 12$, is also overestimated by the Joshi correlation by 25% at $w/d = 15.2$. The formulas of Ref. 16 that were developed for liquid jets and compared very well with the present liquid plume measurements would overestimate the penetration of this slurry jet by 37.5% and the width of 71.6%. Clearly, new correlations for width and penetration must be developed for slurry jets.

Further Results for the $\bar{q} = 6.0$ Liquid Jet

Pressure Distributions

The static pressure P_s is given in parentheses above the total pressure measurements in Fig. 9. Also shown is the average time variation in the total pressure during a run.

The static pressure measurements are probably high by as much as 20-25%. This was found by comparing the measured freestream static pressure of about 1.37×10^4 Pa to the calculated freestream static pressure of about 1.16×10^4 Pa, both without injection. The large percentage results from the low absolute value of static pressure. This error was probably caused by a -3 deg angle of attack of the probe. These are maximum errors because there are small flow inclinations in the still expanding jet that would decrease the effective angle of attack. Thus, the static pressure measurements are presented as collected. The static pressure varied by less than 3.45×10^3 Pa within the jet and differed by less than 3.45×10^3 Pa from the freestream value.

The total pressure measurements show considerable variation from the low values in the center to the freestream values on the boundaries. Of course, the major source of error in the presented values of pitot pressure involves the transfer of the momentum of the liquid particles entering the probe to the air. Thus, using the local velocity of the air as the maximum possible velocity of the liquid particles, the momentum of the liquid divided by the capture area of the probe represents the maximum error. For Mach numbers greater than about 2.0, the measured values were at most 1.5% too high. For Mach numbers less than 1.5, the measured values were high by a maximum of 15% for an average about 8% too high.

Mach Number Distribution

The Rayleigh supersonic pitot formula allows the calculations of the local freestream Mach number once P_{t2}, P_s, and γ are known. If the flow is not supersonic, then M is determined from the isentropic formula using P_{t1}, P_s, and γ. Simple calculations assuming uniform distribution of liquid droplets across the jet plume area show that there is only 0.0001 mm^3 of liquid per 1 mm^3 of jet volume. At these low static temperatures, little liquid vapor can be expected. Thus, the flow is primarily air and, for estimating M inside the jet, γ for air can be reasonably assumed.

The result is shown in Fig. 10. The values on the boundary are high as expected and do not exceed $M = 3$. The Mach numbers decrease smoothly as the center of the jet is approached to quite low values. There is actually a large subsonic region even though this is measured at $x/d = 30$ with a high freestream Mach number. The uncertainty in these Mach numbers is related to the errors in the measured static and pitot pressures, which tend to offset each other in the calculation of Mach number. The calculated values of Mach number in the subsonic region are at most 10% too low and in the supersonic region are at most 5% too low.

The large subsonic region introduces an uncertainty in the mass flow measurements already presented. Without exactly isokinetic sampling, some distortion of the flowfield will exist making the effective capture area different from the actual capture area of the probe. From the possible flow scenarios based on measured pressures, the worst case was determined to be a local $M = 0.6$ with choked flow at the entrance of the probe. This would result in a maximum increase in effective capture area of 17% over the capture area of the probe. It is unlikely that the values of $\dot{m}_l/A$ are as much as 17% too high, however, since the trajectory of droplets approaching the probe will not be altered as dramatically as that of the air.

Jet Plume Core Region

Reference 16 concluded that there were two regions in the jet plume, a peripheral mixing region and a core region. From their temperature survey method they characterized the core as where the measured temperature varied little and the mixing region by marked changes in temperature. Reference 16 obtained the following correlation for the penetration of this core region:

$$h_{\text{core}}/d = 3.17(\bar{q})^{0.414}(x/d)^{0.239}$$

For the present test conditions, this would yield a value of $h_{\text{core}}/d = 15.0$. Figure 6 shows similar trends where there is relatively constant mass flow from $y/d = -4$ to 4 at a given z/d station up to $z/d = 12$. This region has low run-to-run variation in the mass flow samples collected. Figure 9 shows the core region has virtually constant total pressure with no time variation in total pressure. This region also corresponds to the subsonic region as shown in Fig. 10. Thus, there is a clearly defined core region; however, at $x/d = 30$ its penetration is only $h_{\text{core}}/d = 12$ or 25% below the value from the less direct temperature method. The present data also give $w_{\text{core}}/d = 8$. The core region also carries approximately two-thirds of the plume mass flow at $x/d = 30$ or one-half of the total mass flow through the injector, while it occupies only one-third of the plume area.

Peripheral Mixing Region

This region surrounding the core occupies two-thirds of the plume area while carrying only one-third of the plume mass flow. The difference between the high and low samples collected at each station generally becomes a large fraction of the average mass flow sample, which is shown in Fig. 6, in this peripheral region. Figure 9 shows increasing time variation in total pressure measured in the peripheral region as opposed to none in the core. In addition, the solids were collected on the periphery of the slurry jet at irregular intervals. Also, both liquid and slurry jets were found not to be symmetric. Numerous spark schlieren photographs (10^{-6} s exposure) such as shown in Fig. 3 have shown that the top region of the jet is unsteady in its exact location. This action is related to the clump detachment mechanism of the breakup, which has been documented[10] at about 10^4 cycles/s. This type of unsteadiness should not be evident in the 5 s sampling time. It is apparent then that a low-frequency oscillation of the jet exists on the order of 1 cycle/s. A possible mechanism for this would be oscillation of the separation region around the injector. This is most likely because of large variations in the size of the interaction shock caused by this separation region in front of the injector noticed in spark schlieren photographs.

Liquid-to-Air Ratio

The static temperature distribution can be calculated using the Mach number from Fig. 10 and using the isentropic formula where $T_s = f(T_0, \gamma, M)$ since these quantities are known locally. The argument for using γ for air has already been presented and found to yield reasonable results in the Mach number survey. The stagnation temperature T_0 is taken as constant at 300 K, that of the freestream, since the shock or jet should not affect T_0. With this determined, the mass flow of air per unit area can be calculated as

$$\dot{m}_a/A = MP_s\sqrt{\gamma/RT_s}$$

The minimum values of $\dot{m}_a/A$ are reached almost uniformly at $z/d = 8$ for all y/d values. The air mass flow increases sharply for $z/d > 8$, but also increases slightly for $z/d < 8$. An equivalent trend for $\dot{m}_l/A$ is not noticed as $\dot{m}_l/A$ drops smoothly as the surface of the flat plate is approached.

The two mass flow distributions can be combined into a liquid-to-air ratio distribution as shown in Fig. 11. For a typical hydrocarbon fuel, which these liquid tests simulate, stoichiometric fuel-to-air ratio would be approximately 0.1. As can clearly be seen, this condition would occur only in a very narrow band on the periphery of the jet.

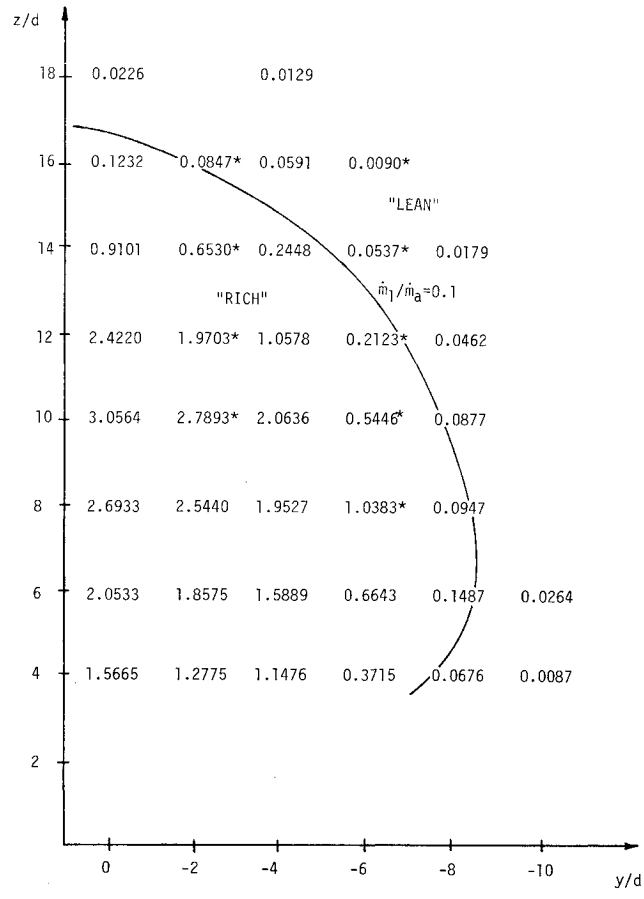

Fig. 11 Calculated liquid-to-air mass flow ratio for the liquid jet (* denotes interpolated P_s values).

Momentum Flux

The velocity of the air, $V_a = M\sqrt{\gamma RT_s}$, is used to calculate the momentum flux of air per unit area, $\dot{m}_a V_a/A$, and both are shown in Fig. 12. Fluxes are seen to drop by about one order of magnitude from the supersonic region to the plume core. This is due to both lower velocity and lower mass flow of air. To calculate a momentum flux for the liquid, an average velocity of the particles would have to be assumed. Certainly, the velocity can be no greater than that of the air, but it could be equal to that of the air this far downstream. However, momentum fluxes calculated on this assumption showed that in the core the momentum flux of liquid would be greater than that of the air, which could not be since the liquid was injected with no axial momentum. Thus, in this region, the air momentum flux can be taken as a limit on the flux of the

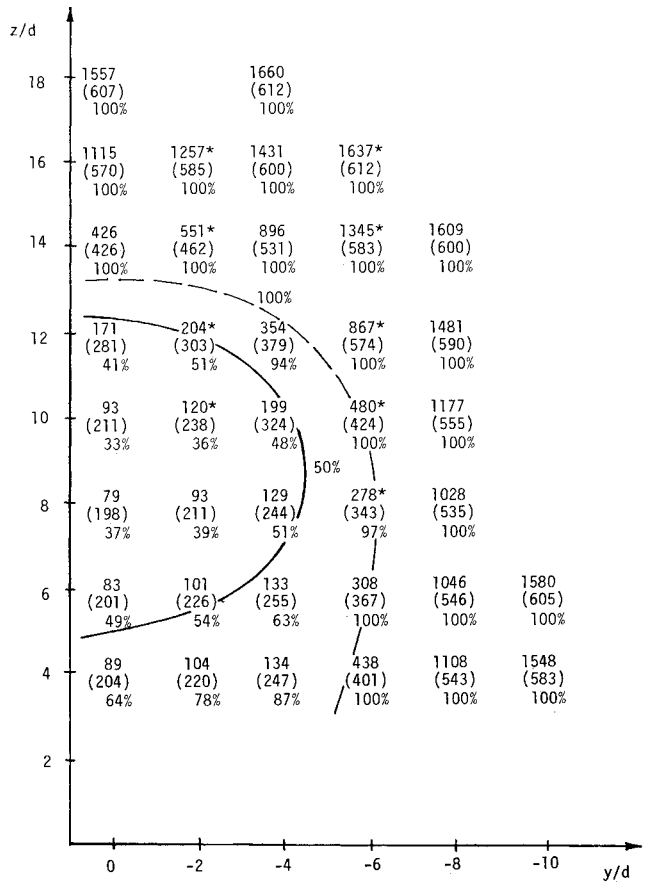

Fig. 12 For the liquid jet, calculated momentum flux of air $\dot{m}_a V_a / A \cdot (10^2)$ g/mm·s^2; velocity of air V_a, m/s, in parentheses; and maximum velocity of liquid as percentage of air velocity (* denotes interpolated P_s values).

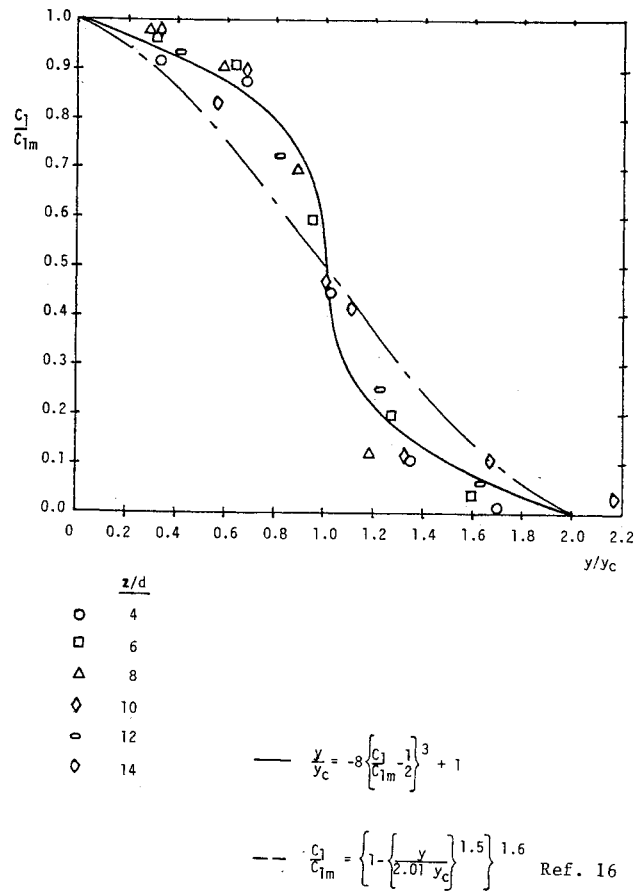

Fig. 13 Liquid concentration data and correlations for $\bar{q} = 6.0$ liquid jet.

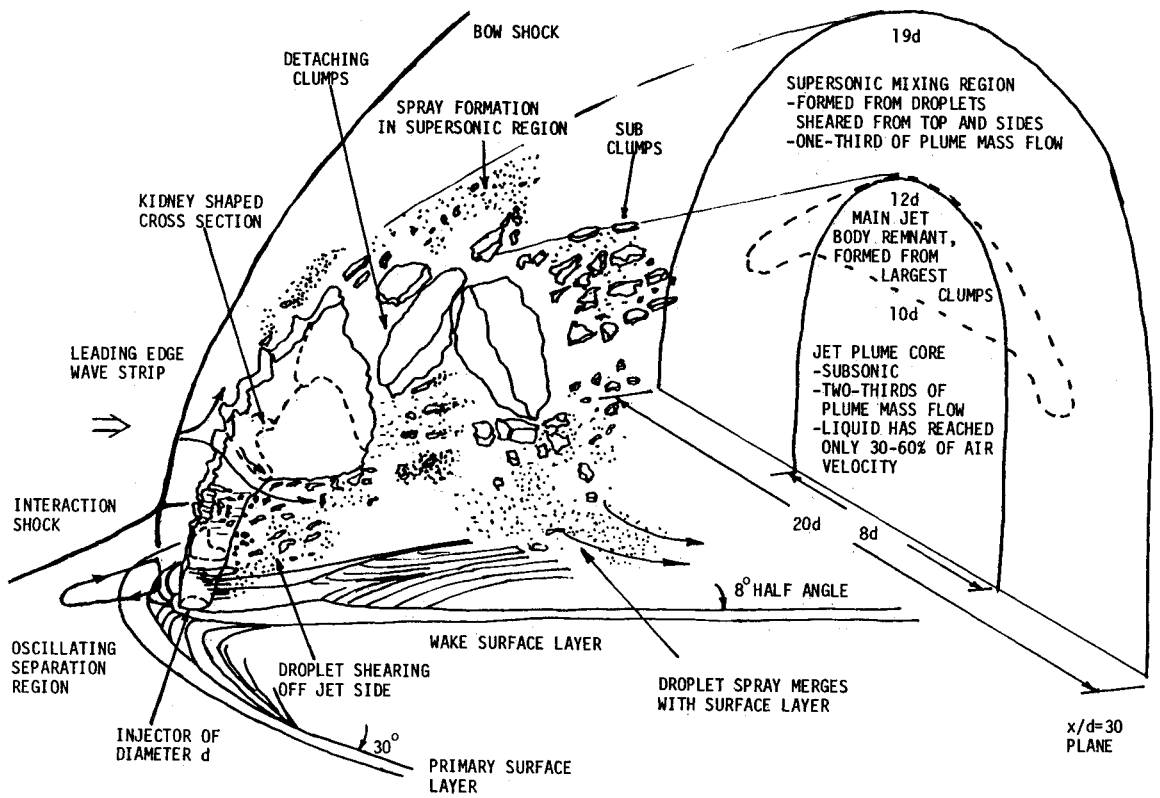

Fig. 14 Flowfield schematic of liquid jet transverse injection in Mach 3.0 airflow from a circular orifice.

liquid. As such, it can also give an upper limit on the velocity of the particles. In Fig. 12, the maximum velocity of the liquid expressed as a percentage of the air velocity at the same location is also shown. At least in this subsonic region, the particles can be traveling at substantially lower velocities than the surrounding air, even though this is at the $x/d = 30$ plane in a $M = 3$ flow. Previous work in a $M = 2$ flow assumed velocity equilibration to within 1% in the vicinity of the injector.[19] It is apparent that even though the jet has lost its normal momentum and is coflowing with the air stream, there is considerable axial momentum left to be transferred to the particles and air in the core from the surrounding supersonic region. Considerable mixing within the jet will occur for a large distance downstream.

Liquid Concentration Correlations

A correlation for the nondimensional liquid concentration in the downstream plane of $x/d = 30$ can be derived as follows. The gas concentration is defined as

$$C_a = \frac{\dot{m}_a/A}{\dot{m}_a/A + \dot{m}_l/A}$$

and the liquid concentration by

$$C_l = \frac{\dot{m}_l/A}{\dot{m}_a/A + \dot{m}_l/A}$$

Thus, the liquid and gas concentrations are related by $C_a + C_l = 1$. Values on the centerline, $y/d = 0$, can be denoted by the subscript m. Also, at a given height z/d the distance from the centerline to a point is y and y_c is the distance from the centerline to the point at which $C_l = \frac{1}{2}C_{l_m}$. The data in the $x/d = 30$ plane are plotted as C_l/C_{l_m} vs y/y_c in Fig. 13.

Using an indirect temperature technique, Shaikhutdinov and Klevanskii[16] performed a similar correlation, but for the concentration only in the plane of symmetry, $y/d = 0$, at various x/d stations. The result was the equation

$$\frac{C_l}{C_{l_m}} = \left[1 - \left(\frac{z}{2.01 z_c}\right)^{1.5}\right]^{1.6}$$

where C_{l_m} was the concentration on a centerline connecting the points of maximum liquid concentration at each x/d plane downstream of the injector. Simply written in terms of y coordinates and applied to the current data in the $x/d = 30$ plane, it does not represent the data well, as can be seen from Fig. 13. The data can be fit well by the cubic equation

$$\frac{y}{y_c} = -8\left(\frac{C_l}{C_{l_m}} - \frac{1}{2}\right)^3 + 1$$

In the absence of further data, this can be taken as an adequate representation for a wide range of downstream stations.

Liquid Jet Synthesis

As a means to synthesize the many aspects of the liquid jet structure, breakup and plume characteristics that have been investigated and described, Fig. 14 is presented as a schematic of the flowfield structure of a $\bar{q} = 6.0$ liquid jet.

Conclusions

This research has contributed data to a sparsely researched area for transversely injected jets into supersonic flow—a mass flow distribution across the jet plume. The conclusions discussed below will hopefully add new insight to jet structure and mixing for both liquid and slurry injectants.

The actual penetration and width of the liquid jet at $x/d = 30$ were approximately 20% above that determined from photographic techniques. A favorable comparison with the published data of another intrusive method indicates that intrusive techniques provide a more accurate determination of jet boundaries. The correlations for liquid jets, however, are not applicable to the penetration and width of slurry jets.

Mass flow data indicate that the slurry and liquid jets are both slightly asymmetrical about the centerline axis. This, along with additional sampling, pressure, and photographic data, indicates that there is a possibility of low-frequency oscillations of the jet in the side-to-side and upstream-downstream direction.

The leading edge of a liquid or slurry jet has been found to have a leading-edge wave strip at least 4-5d high with droplet shearing off the sides. The height of the wave strip is linked to the location of the transition to supersonic flow over the jet. The circular jet probably is distorted early in its penetration into a kidney-shaped cross section, which is still identifiable far downstream, affecting plume distributions of mass flow.

A liquid-to-air ratio distribution calculated in the $x/d = 30$ plane of the liquid jet showed that for simulated fuel and air mixing at least one order of magnitude more air must be mixed with the liquid to bring the ratios close to stoichiometric for a hydrocarbon-air mixture. A correlation for the nondimensional liquid concentration across the plume at a downstream plane has been developed, relating the nondimensional distance from the centerline to the cube of the concentration.

The cross section of the jet plume has at least two clearly defined regions. There is a core region that has high subsonic air velocity and a relatively constant mass flow in the side-to-side direction at a given vertical location along with low total pressure. The largest clumps detached from the main jet body form this core region. As a result, for the liquid jet at 30 injector diameters downstream, the core occupies one-third of the plume area but carries two-thirds of the plume mass flow. The slow acceleration of these large clumps by the subsonic airflow results in the liquid particles having reached only 30-60% of the velocity of the air.

Surrounding the core region is the peripheral mixing region characterized by supersonic velocities, increasing pitot pressures, and decreasing mass flows. The remaining one-third of the mass flow captured in the plume is carried in this region. Droplets sheared off the sides and top of the main jet body are the source of the mass flow in this region. However, because of the high velocity and high air mass flow in this region compared to that in the core, considerable further mixing with and momentum transfer to the core region is anticipated downstream.

A similar structure in the slurry jet is likely. More importantly, substantial phase separation was found. The local loading in the center of the jet was only one-third of the injected value and increased significantly as the boundary of the plume is approached from any direction.

At least two fundamental differences in structure exist between slurry and liquid jets at the tested conditions. First, the half-angle of divergence of the slurry main body is roughly half that of the liquid jet. Second, the wake surface layer of the slurry has a half-angle of divergence 2.5 times that of the liquid.

Acknowledgment

This research was supported in full by the U.S. Air Force Office of Scientific Research. Dr. Julian Tishkoff was Technical Monitor.

References

[1]Yates, C.L. and Rice, J.L., "Liquid Jet Penetration," Applied Physics Laboratory, Johns Hopkins University, Baltimore, Research and Development Programs Quarterly Rept. U-RQR/69-2, 1969.

[2]Kolpin, M.A., Horn, K.P., and Reichenbach, R.E., "Study of Penetration of a Liquid Injectant into a Supersonic Flow," *AIAA Journal*, Vol. 6, May 1968, p. 853.

[3]Forde, J.M., Molder, S., and Szpiro, E.J., "Secondary Liquid Injection into a Supersonic Airstream," *Journal of Spacecraft and Rockets*, Vol. 3, Aug. 1966, p. 1172.

[4]Catton, I., Hill, D.E., and McRae, R.P., "Study of Liquid Jet Penetration in a Hypersonic Stream," *AIAA Journal*, Vol. 6, Nov. 1968, p. 2084.

[5]Reichenbach, R.E. and Horn, K.P., "Investigation of Injectant Properties on Jet Penetration in a Supersonic Stream," *AIAA Journal*, Vol. 9, March 1971, p. 469.

[6]Nejad, A.S. and Schetz, J.A., "Effects of Properties and Location in the Plume on Droplet Diameter for Injection in a Supersonic Stream," *AIAA Journal*, Vol. 21, July 1983, pp. 956-961.

[7]Joshi, P.B. and Schetz, J.A., "Effect of Injector Geometry on the Structure of a Liquid Jet Injected Normal to a Supersonic Air Stream," *AIAA Journal*, Vol. 13, Sept. 1975, pp. 1137-1138.

[8]Hewitt, P.W. and Schetz, J.A., "Atomization of Impinging Liquid Jets in a Supersonic Crossflow," *AIAA Journal*, Vol. 21, Feb. 1983, pp. 178-179.

[9]Kush, E.A. Jr. and Schetz, J.A., "Liquid Jet Injection into Supersonic Flow," *AIAA Journal*, Vol. 11, Sept. 1973, pp. 1223-1224.

[10]Schetz, J.A., Kush, E.A., and Joshi, P.B., "Wave Phenomena in Liquid Jet Breakup in a Supersonic Crossflow," *AIAA Journal*, Vol. 18, July 1980, pp. 774-778.

[11]Olson, W.T. and Setze, P.C., "Some Combustion Problems of High-Energy Fuels for Aircraft," *7th Symposium (International) on Combustion*, Butterworth Scientific Publications, London, 1959, pp. 883-889.

[12]Olson, W.T. and Breitwiser, R., "NACA Research on Slurry Fuels Through 1954," NACA RM E55B14, 1954.

[13]King, M.K., "Ignition and Combustion of Boron Particles and Clouds," *Journal of Spacecraft and Rockets*, Vol. 19, July-Aug. 1982, pp. 294-306.

[14]Less, D. and Schetz, J.A., "Penetration and Break-Up of Slurry Jets in a Supersonic Stream," *AIAA Journal*, Vol. 21, July 1983, pp. 1045-1046.

[15]Yang, M.L., Gu, S.J., Liu, G.E., and Li, X.Y., "Trajectory with Diffusion Method for Predicting the Fuel Distribution in a Transverse Stream," AIAA Paper 83-0336, 1983.

[16]Shaikhutdinov, Z.G. and Klevanskii, V.M., "Penetration and Mixing of Liquid Injected into Supersonic Transverse Gas Stream," *Izvestiya Vysshikh Uchebnykh Zavedenii Aviatsionnaya Tekhnika (Soviet Aeronautics)*, Vol. 19, No. 1, 1976, pp. 99-108.

[17]Abramovich, G.N., *The Theory of Turbulent Jets*, Massachusetts Institute of Technology Press, Cambridge, 1963.

[18]Shaikhutdinov, Z.G., Klevanskii, V.M., Nadyrshin, A.Ya. and Shaikhinurova, L.F., *Izvestiya Vysshikh Uchebnykh Zavedenii, Aviatsionnaya Tekhnika (Soviet Aeronautics)*, No. 4, 1973.

[19]Edelman, R.B., Schmotolochen, S., and Slutsky, S., "Combustion of Liquid Hydrocarbons in a High-Speed Airstream," *AIAA Journal*, Vol. 9, July 1971, pp. 1357-1364.